

Nonlinear vibration of iced cable under wind excitation using three-degree-of-freedom model

Wei Zhang(张伟), Ming-Yuan Li(李明远), Qi-Liang Wu(吴启亮), and An Xi(袭安)
Citation: Chin. Phys. B, 2021, 30 (**9**): 090503. DOI: 10.1088/1674-1056/abea83
Journal homepage: http://cpb.iphy.ac.cn; http://iopscience.iop.org/cpb

What follows is a list of articles you may be interested in

Nonlinear dynamics of a classical rotating pendulum system with multiple excitations

Ning Han(韩宁) and Pei-Pei Lu(鲁佩佩)
Chin. Phys. B, 2020, 29 (**11**): 110502. DOI: 10.1088/1674-1056/ab9df2

Bifurcation and chaos characteristics of hysteresis vibration system of giant magnetostrictive actuator

Hong-Bo Yan(闫洪波), Hong Gao(高鸿), Gao-Wei Yang(杨高炜), Hong-Bo Hao(郝宏波), Yu Niu(牛禹), Pei Liu(刘霈)
Chin. Phys. B, 2020, 29 (**2**): 020504. DOI: 10.1088/1674-1056/ab65b4

Phase order in one-dimensional piecewise linear discontinuous map

Ru-Hai Du(杜如海), Sheng-Jun Wang(王圣军), Tao Jin(金涛), Shi-Xian Qu(屈世显)
Chin. Phys. B, 2018, 27 (**10**): 100502. DOI: 10.1088/1674-1056/27/10/100502

Hysteresis-induced bifurcation and chaos in a magneto-rheological suspension system under external excitation

Hailong Zhang(张海龙), Enrong Wang(王恩荣), Fuhong Min(闵富红), Ning Zhang(张宁)
Chin. Phys. B, 2016, 25 (**3**): 030503. DOI: 10.1088/1674-1056/25/3/030503

Chaotic dynamics and its analysis of Hindmarsh–Rose neurons by Shil'nikov approach

Wei Wei, Zuo Min
Chin. Phys. B, 2015, 24 (**8**): 080501. DOI: 10.1088/1674-1056/24/8/080501

Nonlinear vibration of iced cable under wind excitation using three-degree-of-freedom model*

Wei Zhang(张伟)[1,2,†,‡], Ming-Yuan Li(李明远)[1,2,†], Qi-Liang Wu(吴启亮)[3,§], and An Xi(袭安)[4]

[1] *Beijing Key Laboratory of Nonlinear Vibrations and Strength of Mechanical Structures, Beijing University of Technology, Beijing* 100124, *China*
[2] *College of Mechanical Engineering, Beijing University of Technology, Beijing* 100124, *China*
[3] *School of Artificial Intelligence, Tiangong University, Tianjin* 300387, *China*
[4] *The Fifth Electronic Research Institute of MIIT, Guangzhou* 510610, *China*

(Received 23 November 2020; revised manuscript received 25 January 2021; accepted manuscript online 1 March 2021)

High-voltage transmission line possesses a typical suspended cable structure that produces ice in harsh weather. Moreover, transversely galloping will be excited due to the irregular structure resulting from the alternation of lift force and drag force. In this paper, the nonlinear dynamics and internal resonance of an iced cable under wind excitation are investigated. Considering the excitation caused by pulsed wind and the movement of the support, the nonlinear governing equations of motion of the iced cable are established using a three-degree-of-freedom model based on Hamilton's principle. By the Galerkin method, the partial differential equations are then discretized into ordinary differential equations. The method of multiple scales is then used to obtain the averaged equations of the iced cable, and the principal parametric resonance-1/2 subharmonic resonance and the 2:1 internal resonance are considered. The numerical simulations are performed to investigate the dynamic response of the iced cable. It is found that there exist periodic, multi-periodic, and chaotic motions of the iced cable subjected to wind excitation.

Keywords: iced cable, wind excitation, galloping, chaotic motion

PACS: 05.45.–a, 82.40.Bj **DOI:** 10.1088/1674-1056/abea83

1. Introduction

The nonlinear statics, dynamics, and stability of cables have received considerable attention due to their extensive applications in the engineering field. High-voltage transmission lines are a flexible cable structure widely used in transmission engineering due to their ability to conduct power over long distances. Cable dynamics have a rich history, which has been summarized in the review articles by Irvine and Caughey,[1] Starossek,[2] and Rega and Ibrahim.[3–5] Among all the different types of cable structures, the suspended cable is a fundamental type used in theoretical studies, and exhibits various dynamic phenomena as a prototype model in applied mechanics.

The nonlinear dynamic responses of elastic suspended cables due to finite vibration amplitudes have received considerable research attention, as suspended cables exhibit a variety of phenomena due to their high flexibility and low damping characteristics. Perkins[6] derived a continuum model that describes the nonlinear, three-dimensional response of an elastic cable to tangential oscillations of one support. A two-degree-of-freedom approximation was used to examine the coupled in-plane and out-of-plane response. Additionally, a four-degree-of-freedom model was developed from the continuum equations by Benedettini *et al.*,[7] and is able to capture the main phenomena that are likely to occur in the non-planar finite dynamics of an elastic suspended cable subjected to external force and support motion. Gattulli *et al.*[8] used analytical and finite element models to study the modal interactions in both planar and spatial responses to harmonic in-plane and out-of-plane loads. Luongo *et al.*[9,10] derived a nonlinear model of a twisted cable and studied the effect of the twist angle on the nonlinear galloping of suspended cables. Luongo *et al.*[11] also established a nonlinear two-degree-of-freedom model to describe a flexible elastic suspended cable undergoing galloping oscillations. Kim and Perkins[12] investigated the resonant responses of suspended elastic cables driven by a steady current. Srinil and Rega[13] presented a model formulation capable of reflecting the large-amplitude free vibrations of a suspended cable in three dimensions. Based on a multi-degree-of-freedom model, numerical procedures were implemented to solve both spatial and temporal problems. Zhao and Wang[14] investigated the nonlinear responses of suspended homogeneous elastic cables with low initial sag-to-span ratio in the case of 3:1 internal resonance by considering the vertical load. Casciati and Ubertini[15] considered the nonlinear vibration of shallow cables equipped with a semi-active control de-

*Project supported by the National Natural Science Foundation of China (Grant Nos. 11290152, 11427801, and 11902220) and the Funding Project for Academic Human Resources Development in Institutions of Higher Learning under the Jurisdiction of Beijing Municipality, China (PHRIHLB).

†These authors contributed equally to this work.
‡Corresponding author. E-mail: sandyzhang0@yahoo.com
§Corresponding author. E-mail: qiliang_wu@hotmail.com

© 2021 Chinese Physical Society and IOP Publishing Ltd

vice. Abdel-Rohman and Spencer[16] studied the along-wind and across-wind responses of suspended cables. Zheng *et al.*[17] investigated the super-harmonic and internal resonance characteristics of a viscously damped cable with nearly commensurable natural frequencies via a novel method. Chang *et al.*[18] studied the nonlinear interaction of the first two in-plane modes of a suspended cable with a moving fluid along the plane of the cable. Ouni and Kahla[19] investigated the nonlinear dynamics of a cable under first- and second-order parametric excitations. Zhao *et al.*[20,21] investigated the approximate series solutions of nonlinear free vibrations of suspended cables via the Lindstedt–Poincaré method and the homotopy analysis method.

Owing to the combination of quadratic and cubic nonlinearities, suspended cables exhibit various planar and nonplanar internal resonance conditions. Srinil *et al.*[22] and Srinil and Rega[23] conducted an analytical investigation of resonant multimodal dynamics resulting from 2:1 internal resonance in the finite-amplitude free vibrations of horizontal/inclined cables. Nayfeh *et al.*[24] investigated the nonlinear, nonplanar responses of suspended cables subjected to external excitation. Lacarbonara and Rega[25] investigated 1:1, 2:1, 3:1, and internal resonances in undamped, unforced, one-dimensional systems with arbitrary linear, quadratic, and cubic nonlinearities for a class of shallow symmetric structural systems. Kamel and Hamed[26] studied the nonlinear behavior of an elastic cable subjected to harmonic excitation. Rega *et al.*[27] studied an experimental model of an elastic cable carrying eight concentrated masses and hanging from in-phase or out-of-phase vertically-moving supports. Zhang and Tang[28] investigated the chaotic dynamics and global bifurcations[29–31] of a suspended elastic cable under combined parametric and external excitations. Considering 1:1 internal resonance, Abe[32] investigated the accuracy of nonlinear vibration analyses of suspended cables that possess quadratic nonlinearity and cubic nonlinearity, respectively. By the Galerkin method, Huang *et al.*[33] derived the governing equations describing the motion of a coupled suspended cable-stayed beam structure, and studied its 1:2 internal resonance. Taking into account the bending stiffness, Kang *et al.*[34,35] systematically investigated the linear and nonlinear dynamics of a suspended cable.

Considering the effect of the geometric nonlinearity of the cable on the coupled behavior between the modes of the beam and cable, Wei *et al.*[36] developed and investigated a model of the cable-stayed beam system. Wu and Qi studied the dynamic responses of an iced suspended cable were investigated[37] by the finite element method. Jing *et al.*[38] proposed a numerical model of a wind-loaded two-dimensional (2D) cable, and analyzed the vibration responses induced by rain-wind. The bases of the flow behavior and phenomena existing during 2D airflow were explained by Gorski *et al.*[39] to analyze the motions of an ice-accreted bridge cable. Via the use of the optimal equivalent control algorithm, Zhao *et al.*[40] studied a method of controlling the vibration responses of a stay cable. Chang *et al.*[41] reported experimental results of the mechanism and mitigation of the vibrations of stay cables under rain-wind load. Electromagnetic inertial mass dampers were considered by Li *et al.*[42] to experimentally and analytically study the vibration mitigation of stay cables.

In recent years, some investigations of suspended cable models and research methods have been updated. Using the method of multiple scales, Huang *et al.*[43] developed a new nonlinear partial differential equation to investigate a suspended cable-stayed beam structure by considering the finite deformations of the structure and the initial configuration of the main cable. Ahmad *et al.*[44] established an analytical model of a hybrid system composed of two parallel taut cables interconnected by a transverse linear flexible cross-tie. Ishihara and Oka[45] studied the aerodynamic coefficients of a single bundled iced suspension cable and four bundled iced suspension cables for comparison with the results of a wind tunnel test. Akkaya and Horssen[46] described a model of the rain-wind-induced oscillations of an inclined cable. Based on the mode superposition method with enhanced shape functions, Javanbakht *et al.*[47] proposed a control-oriented numerical model to evaluate the dynamic response of a stay cable. Li *et al.*[48] established a generalized gust loading model for predicting the buffeting response, which is applicable to both small-aspect-ratio and long-span, line-like bridges. Guo *et al.*[49] proposed an elastic cable-rigid body coupled model to investigate the dynamic interaction between the torsional dynamics of the boundary tower and the nonlinear transversal vibrations of the cables. According to catenary theory, Mansour *et al.*[50] studied the free undamped vibration of a suspension cable with arbitrary sag and inclination. Zhao *et al.*[51,52] investigated the influence of the temperature on the vibration characteristics of suspension cables related to the excitation amplitude and sag-to-span ratio, and the results revealed that temperature variation gave rise to qualitative and/or quantitative changes of the nonlinear vibration properties.

The present study focuses on the complex nonlinear vibrations of a three-degree-of-freedom iced cable. The influences of the support displacement and wind excitation on the nonlinear dynamic responses of the system are analyzed. Considering the galloping of the suspended structure under transverse wind, a nonlinear dynamic model of the three-degree-of-freedom iced cable is established. The nonlinear partial differential equations of motion for the iced cable are established via Hamilton's principle. Additionally, the dimensionless differential equations of motion are obtained and reduced into a set of nonlinear ordinary differential equations by the Galerkin method.[53,54] With the assistance of the method of multiple

scales, the averaged equations of the system in the presence of principal parametric resonance $-1/2$ subharmonic resonance and 2:1 internal resonance are obtained. According to the averaged equations, the numerical results including bifurcation diagrams, waveforms, phase plots, and frequency spectrum are obtained to investigate the intrinsically nonlinear behaviors of the iced cable. It is demonstrated that the iced cable exhibits alternating periodic and chaotic motions according to the influences of the nonlinear factors.

2. Theory and formulation

Transversely galloping will be excited because the irregular section of an iced cable alternately results in changes in lift and drag. Figure 1 defines the coordinate system of a three-degree-of-freedom iced cable. The natural coordinate system is established along the axis of the cable, in which U_1, U_2, and U_3 are the displacements of the cable in the tangent, normal, and auxiliary directions, respectively. The displacement of the left support along the cable is $U_{\rm m}\cos\bar{\Omega}_1 t$. The transverse wind speed can be expressed as $V_{\rm W}=\bar{V}+V_{\rm m}\sin\Omega_2 t$.

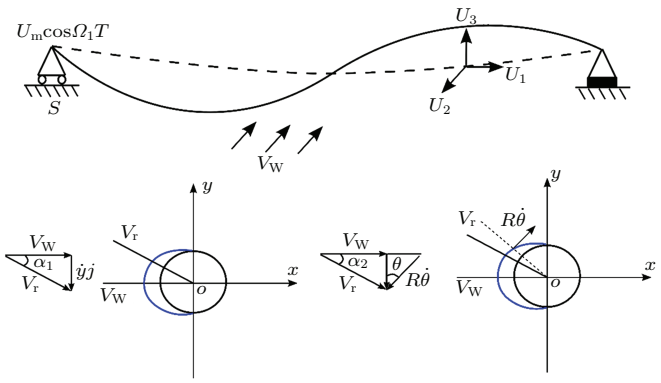


Fig. 1. Model of iced cable.

Considering the interception of a small section of the iced cable for centralized mass, the center of mass of the line lies on the origin O. In the Cartesian coordinate (oxy) system, the vertical coordinate of the center of mass is y. For a wind speed $V_{\rm m}$, the relative velocity is $V_{\rm r}=V_{\rm w}-\dot{y}\boldsymbol{j}$, where $\boldsymbol{j}$ is the unit vector along the y axis. Let α_1 be the angle of attack caused by the vertical motion of the cable, let α_2 be the angle of attack caused by the suspension of the cable, and let θ be the cable rotation angle:

$$\alpha_1=-\frac{\dot{y}}{V_{\rm W}},\quad \alpha_2=-\frac{\dot{u}_4}{V_{\rm W}}, \tag{1}$$

then the angle of attack α will be

$$\alpha=-\frac{\dot{y}+\dot{u}_4}{V_{\rm W}}. \tag{2}$$

Because the cross-section of the iced cable is a non-circular irregular shape, the gust of the suspension produces not only a resistance $F_{\rm d}$ in the $V_{\rm r}$ direction, but also a lift $F_{\rm L}$ and a torsional force $F_{\rm w}$ that are perpendicular to it. According to the aerodynamic principle, the following equations can be obtained:

$$F_{\rm L}(T)=\frac{1}{2}\rho_{\rm air}V_{\rm W}^2 dC_{\rm L}, \tag{3a}$$

$$F_{\rm d}(T)=\frac{1}{2}\rho_{\rm air}V_{\rm W}^2 dC_{\rm D}, \tag{3b}$$

$$F_{\rm w}(T)=\frac{1}{2}\rho_{\rm air}V_{\rm W}^2 dC_{\rm M}. \tag{3c}$$

The tangential force and normal force of the cable are respectively

$$F_2=F_{\rm L}\cos\alpha-F_{\rm d}\sin\alpha, \tag{4a}$$

$$F_3=F_{\rm L}\sin\alpha-F_{\rm d}\cos\alpha. \tag{4b}$$

Because the model considers low-frequency vibration, the value of α is very small; thus, the following approximate expressions can be held:

$$\cos\alpha\approx\alpha,\quad \sin\alpha\approx\frac{\dot{y}+\dot{u}_4}{V_{\rm W}}. \tag{5}$$

By substituting Eqs. (2), (3), and (5) into Eq. (4), the effects of the wind along the cable in the tangential, normal, and rotational directions of the component can be calculated, respectively, as

$$F_2(T)=\frac{1}{2}\rho_{\rm air}V_{\rm W}^2 dC_{\rm L}-\frac{1}{2}\rho_{\rm air}V_{\rm W}^2 dC_{\rm D}\frac{\dot{y}+\dot{u}_4}{V_{\rm W}}, \tag{6a}$$

$$F_3(T)=\frac{1}{2}\rho_{\rm air}V_{\rm W}^2 dC_{\rm D}-\frac{1}{2}\rho_{\rm air}V_{\rm W}^2 dC_{\rm L}\frac{\dot{y}+\dot{u}_4}{V_{\rm W}}, \tag{6b}$$

$$F_4(T)=\frac{1}{2}\rho_{\rm air}V_{\rm W}^2 dC_{\rm M}, \tag{6c}$$

where d is the maximum dimension of the aerial surface of the cable, and $C_{\rm L}$, $C_{\rm D}$, and $C_{\rm M}$ are respectively the lift, drag, and torsional coefficients, which are the functions of the cross-sectional shape and the angle of attack.

According to Hamilton's principle,

$$\delta\left[\int_{T_2}^{T_1}(\Pi_{\rm T}-\Pi_{\rm S}+\Pi_{\rm W})\,{\rm d}T\right]=0, \tag{7}$$

where Π_T, $\Pi_{\rm S}$, and $\Pi_{\rm W}$ are the kinetic energy, strain energy, and external force work, respectively. The equations of motion can be obtained by applying Hamilton's principle as follows:

$$\frac{\partial}{\partial S}\left[(P+EA\varepsilon_{\rm d})\left(1+\frac{\partial U_1}{\partial S}-KU_2\right)\right]-(P+EA\varepsilon_{\rm d})K\left(\frac{\partial U_1}{\partial S}-KU_2\right)-\rho g\sin\beta=\rho\frac{\partial^2 U_1}{\partial T^2}, \tag{8a}$$

$$\frac{\partial}{\partial S}\left[(P+EA\varepsilon_{\rm d})\left(1+\frac{\partial U_2}{\partial S}-KU_1\right)\right]-(P+EA\varepsilon_{\rm d})K\left(\frac{\partial U_1}{\partial S}-KU_2\right),$$

$$-\rho g\cos\beta+\frac{1}{2}\rho_{\rm air}V_{\rm W}^2 dC_{\rm L}-\frac{1}{2}\rho_{\rm air}V_{\rm W}C_{\rm D}(\dot{y}+\dot{u}_4)=\rho\frac{\partial^2 U_1}{\partial T^2}, \tag{8b}$$

$$\frac{\partial}{\partial S}\left[(P+EA\varepsilon_{\rm d})\frac{\partial U_3}{\partial S}\right]+\frac{1}{2}\rho_{\rm air}V_{\rm W}^2 dyC_{\rm D}+\frac{1}{2}\rho_{\rm air}V_{\rm W}dC_{\rm L}(\dot{y}+\dot{u}_4)=\rho\frac{\partial^2 U_3}{\partial T^2}, \tag{8c}$$

$$\frac{\partial}{\partial S}(M_0+B_T\varepsilon_{\rm d}+GJ\varepsilon_\theta)+\frac{1}{2}\rho_{\rm air}V_{\rm W}^2 d^2C_{\rm M}=J_{\rm c}\frac{\partial^2 U_4}{\partial T^2}. \tag{8d}$$

The boundary conditions of the cable are given as

$$U_1(0,T)=U_{\rm m}\sin\Omega_1 T,\quad U_1(L,T)=0, \tag{9a}$$

$$U_2(0,T)=0,\quad U_2(L,T)=0, \tag{9b}$$

$$U_3(0,T)=0,\quad U_3(L,T)=0. \tag{9c}$$

The tension and curvature expressions are respectively

$$P(S)=\sqrt{P^2+\left[\rho g\left(S-\frac{L}{2}\right)\right]^2}, \tag{10a}$$

$$K(S)=\frac{\rho g P_0}{P_0^2+\left[\rho g\left(S-\frac{L}{2}\right)\right]^2}, \tag{10b}$$

where

$$P_0=\frac{\rho gLH}{8D}. \tag{11}$$

Equation (11) shows that when the sag-to-span ratio$D/H\le 1/8$, $P_0\ge\rho gL$. By taking the Taylor expansion of Eq. (10), the following equation is obtained:

$$P=P_0,\quad K=\frac{\rho g}{P_0}. \tag{12}$$

The dimensionless curvature is $k=KL=\rho gL/P_0$, and can be regarded as a small perturbation parameter. By expanding Eq. (8) and omitting k^2 and higher-order terms, the dynamic equations of small sag are obtained as follows:

$$\frac{\partial}{\partial S}\left(EA\left\{\frac{\partial U_1}{\partial S}-KU_2+\frac{1}{2}\left[\left(\frac{\partial U_2}{\partial S}\right)^2+\left(\frac{\partial U_3}{\partial S}\right)^2\right]\right\}\right)=\rho\frac{\partial^2 U_1}{\partial T^2}, \tag{13a}$$

$$\frac{\partial}{\partial S}\left(P_0+EA\left\{\frac{\partial U_1}{\partial S}-KU_2+\frac{1}{2}\left[\left(\frac{\partial U_2}{\partial S}\right)^2+\left(\frac{\partial U_3}{\partial S}\right)^2\right]\right\}\right)\frac{\partial U_2}{\partial S}$$
$$+KEA\left\{\frac{\partial U_1}{\partial S}-KU_2+\frac{1}{2}\left[\left(\frac{\partial U_2}{\partial S}\right)^2+\left(\frac{\partial U_3}{\partial S}\right)^2\right]\right\}+\frac{1}{2}\rho_{\rm air}V_{\rm W}^2 dC_{\rm L}-\frac{1}{2}\rho_{\rm air}V_{\rm W}dC_{\rm D}(\dot{y}+\dot{u}_4)=\rho\frac{\partial^2 U_2}{\partial T^2}, \tag{13b}$$

$$\frac{\partial}{\partial S}\left(P_0+EA\left\{\frac{\partial U_1}{\partial S}-KU_2+\frac{1}{2}\left[\left(\frac{\partial U_2}{\partial S}\right)^2+\left(\frac{\partial U_3}{\partial S}\right)^2\right]\right\}\right)\frac{\partial U_3}{\partial S}+\frac{1}{2}\rho_{\rm air}V_{\rm W}^2 dC_{\rm D}-\frac{1}{2}\rho_{\rm air}V_{\rm W}dC_{\rm L}(\dot{y}+\dot{u}_4)=\rho\frac{\partial^2 U_3}{\partial T^2}, \tag{13c}$$

$$\frac{\partial}{\partial S}\left(B_T\left\{\frac{\partial U_1}{\partial S}-KU_2+\frac{1}{2}\left[\left(\frac{\partial U_2}{\partial S}\right)^2+\left(\frac{\partial U_3}{\partial S}\right)^2\right]\right\}+GJ\frac{\partial U_4}{\partial S}\right)+\frac{1}{2}\rho_{\rm air}\left(\bar{V}+V_{\rm m}\sin\bar{\Omega}_2 T\right)d^2C_{\rm M}=J_{\rm c}\frac{\partial^2 U_4}{\partial T^2}. \tag{13d}$$

To obtain the dimensionless governing equation of motion, the transformations of the variables and parameters are introduced as

$$s=\frac{S}{L},\quad t=\frac{T}{\sqrt{L/g}},\quad k=\frac{\rho gL}{P_0},$$
$$v_{\rm t}^2=\frac{P_0}{\rho gL}=\frac{1}{k},\quad u_i=\frac{U_i}{L}\quad (i=1,2,3,4), \tag{14a}$$
$$v_l^2=\frac{EA}{\rho gL},\quad v_{\rm m}^2=\frac{B_T}{\rho gL},\quad v_{\rm b}^2=\frac{B_T}{J_{\rm c}gL},$$

$$v_{\rm n}^2=\frac{GJ}{J_{\rm c}gL},\quad w_l^2=\frac{\rho_{\rm air}d(C_{\rm L}-C_{\rm D})}{2\rho g}, \tag{14b}$$
$$w_{\rm d}^2=\frac{\rho_{\rm air}d(C_{\rm L}+C_{\rm D})}{2\rho g},\quad w_{\rm m}^2=\frac{\rho_{\rm air}d^2C_{\rm M}}{2J_{\rm c}g},$$
$$\Omega_2=\bar{\Omega}_2\sqrt{\frac{L}{g}}. \tag{14c}$$

Substitution of these parameters into Eq. (13) yields the following equations:

$$\frac{\partial}{\partial s}\left(v_l^2\left\{\frac{\partial u_1}{\partial s}-ku_2+\frac{1}{2}\left[\left(\frac{\partial u_2}{\partial s}\right)^2+\left(\frac{\partial u_3}{\partial s}\right)^2\right]\right\}\right)=\rho\frac{\partial^2 u_1}{\partial t^2}, \tag{15a}$$

$$\frac{\partial}{\partial s}\left(v_{\mathrm{t}}^2+v_l^2\left\{\frac{\partial u_1}{\partial s}-ku_2+\frac{1}{2}\left[\left(\frac{\partial u_2}{\partial s}\right)^2+\left(\frac{\partial u_3}{\partial s}\right)^2\right]\right\}\right)\frac{\partial u_2}{\partial s}$$

$$+kv_l^2\left\{\frac{\partial u_1}{\partial s}-ku_2+\frac{1}{2}\left[\left(\frac{\partial u_2}{\partial s}\right)^2+\left(\frac{\partial u_3}{\partial s}\right)^2\right]\right\}+w_l^2V_{\mathrm{W}}^2-w_{\mathrm{d}}^2V_{\mathrm{W}}\left(\frac{\partial u_2}{\partial t}+\frac{\partial u_4}{\partial t}\right)=\rho\frac{\partial^2u_2}{\partial t^2}, \tag{15b}$$

$$\frac{\partial}{\partial s}\left(v_{\mathrm{t}}^2+v_l^2\left\{\frac{\partial u_1}{\partial s}-ku_2+\frac{1}{2}\left[\left(\frac{\partial u_2}{\partial s}\right)^2+\left(\frac{\partial u_3}{\partial s}\right)^2\right]\right\}\right)\frac{\partial u_3}{\partial s}+w_{\mathrm{d}}^2V_{\mathrm{W}}^2-w_{\mathrm{d}}^2V_{\mathrm{W}}\left(\frac{\partial u_2}{\partial t}+\frac{\partial u_4}{\partial t}\right)=\rho\frac{\partial^2u_3}{\partial t^2}, \tag{15c}$$

$$\frac{\partial}{\partial s}\left(v_{\mathrm{b}}^2\left\{\frac{\partial u_1}{\partial s}-ku_2+\frac{1}{2}\left[\left(\frac{\partial u_2}{\partial s}\right)^2+\left(\frac{\partial u_3}{\partial s}\right)^2\right]\right\}+v_{\mathrm{n}}^2\frac{\partial u_4}{\partial s}\right)+V_{\mathrm{W}}^2=\frac{\partial^2u_4}{\partial t^2}. \tag{15d}$$

Because the vibration in the tangential direction of the suspension cable does not play a major role, the vibration in the L_1 direction is ignored, which yields

$$\frac{\partial u_1}{\partial s}-ku_2+\frac{1}{2}\left[\left(\frac{\partial u_2}{\partial s}\right)^2+\left(\frac{\partial u_3}{\partial s}\right)^2\right]=g(t), \tag{16}$$

therefore,

$$u_1(s,t)=u_{\mathrm{m}}\cos\Omega_1t+g(t)s+\int_0^s\left[ku_2(\eta,t)-\frac{1}{2}\left\{\left[\frac{\partial u_2(\eta,t)}{\partial\eta}\right]^2+\left[\frac{\partial u_3(\eta,t)}{\partial\eta}\right]^2\right\}\right]\mathrm{d}\eta, \tag{17}$$

where

$$g(t)=-u_{\mathrm{m}}\cos\Omega_1t+\int_0^l\left[-ku_2(\eta,t)-\frac{1}{2}\left\{\left[\frac{\partial u_2(\eta,t)}{\partial\eta}\right]^2+\left[\frac{\partial u_3(\eta,t)}{\partial\eta}\right]^2\right\}\right]\mathrm{d}\eta, \tag{18}$$

$$u_{\mathrm{m}}=\frac{U_{\mathrm{m}}}{L},\quad \Omega_1=\bar{\Omega}_1\sqrt{\frac{L}{g}}. \tag{19}$$

Substitution of Eq. (17) into Eq. (15) yields the following equations:

$$\left[v_{\mathrm{t}}^2+v_l^2g(t)+v_{\mathrm{m}}^2\frac{\partial u_4}{\partial s}\right]\frac{\partial^2u_2}{\partial s^2}$$

$$+\left[kv_l^2g(t)+v_{\mathrm{m}}^2\frac{\partial u_4}{\partial s}\right]+w_l^2V_{\mathrm{W}}^2$$

$$-w_{\mathrm{d}}^2V_{\mathrm{W}}\left(\frac{\partial u_2}{\partial t}+\frac{\partial u_4}{\partial t}\right)=\frac{\partial^2u_2}{\partial t^2}, \tag{20a}$$

$$\left[v_{\mathrm{t}}^2+v_l^2g(t)+v_{\mathrm{m}}^2\frac{\partial u_4}{\partial s}\right]\frac{\partial^2u_3}{\partial s^2}$$

$$+w_{\mathrm{d}}^2V_{\mathrm{W}}^2-w_l^2V_{\mathrm{W}}\left(\frac{\partial u_2}{\partial t}+\frac{\partial u_4}{\partial t}\right)=\frac{\partial^2u_3}{\partial t^2}, \tag{20b}$$

$$v_{\mathrm{n}}^2\frac{\partial^2u_4}{\partial s^2}+w_{\mathrm{m}}^2V_{\mathrm{W}}^2=\frac{\partial^2u_4}{\partial t^2}. \tag{20c}$$

The boundary conditions are given as

$$u_2(0,t)=0,\quad u_2(1,t)=0, \tag{21a}$$

$$u_3(0,t)=0,\quad u_3(1,t)=0. \tag{21b}$$

The Galerkin method is used to separate the variables, and the partial differential equations are then transformed into ordinary differential equations:

$$u_2(s,t)=v_2(t)\theta_{2i}(s), \tag{22a}$$

$$u_3(s,t)=v_3(t)\theta_{3j}(s), \tag{22b}$$

$$u_4(s,t)=v_4(t)\theta_{4m}(s). \tag{22c}$$

The in-plane vibration mode is as follows:

$$\theta_{2i}=\sqrt{2}\sin i\pi s,\quad i=2,4,6,\ldots, \tag{23a}$$

$$\omega_2=i\pi v,\quad i=2,4,6,\ldots, \tag{23b}$$

$$\theta_{2i}=\frac{2Q}{\cos(\omega_2/2v_{\mathrm{t}})}\sin\frac{\omega_2}{2v_{\mathrm{t}}}\sin\frac{\omega_2(s-1)}{2v_{\mathrm{t}}},\ i=1,3,5,\ldots, \tag{23c}$$

with

$$Q=\sqrt{\frac{\frac{\omega_2}{v_{\mathrm{t}}}\left(1+\cos\frac{\omega_2}{v_{\mathrm{t}}}\right)}{\frac{\omega_2}{v_{\mathrm{t}}}\left(2+\cos\frac{\omega_2}{v_{\mathrm{t}}}-3\sin\frac{\omega_2}{v_{\mathrm{t}}}\right)}}, \tag{24}$$

where ω is determined by the following characteristic equation:

$$\tan\frac{\omega_2}{2v_{\mathrm{t}}}-\frac{1}{2}\left[\frac{\omega_2}{v_{\mathrm{t}}}-\frac{\left(\frac{\omega_2}{v_{\mathrm{t}}}\right)^3}{\frac{v_l^2}{\left(v_{\mathrm{t}}^2\right)^3}}\right]=0. \tag{25}$$

The out-of-plane vibration mode is as follows:

$$\theta_{3m}=\sqrt{2}\sin m\pi s,\quad m=1,2,3,\ldots, \tag{26a}$$

$$\omega_3 = m\pi v_t, \quad m = 1,2,3,\ldots. \tag{26b}$$

The torsional mode is

$$\theta_{4n} = \sqrt{2}\sin n\pi s, \quad n = 1,2,3,\ldots, \tag{27a}$$

$$\omega_4 = n\pi v_n, \quad n = 1,2,3,\ldots. \tag{27b}$$

By applying the Galerkin procedure to the dimensionless governing differential equation of motion, *i.e.*, by substituting Eqs. (22)–(27) into Eq. (20), the three-degree-of-freedom ordinary differential equations of the cable motion are obtained as follows:

$$\begin{aligned}&\ddot{v}_2 + \omega_2^2 v_2 + \mu_1 V_W \dot{v}_2 + \mu_2 V_W \dot{v}_4\\ &-(p_2 u_m \cos\Omega_1 t)\, v_2 + \beta_1 v_2 v_3^2 + \beta_2 v_2^3 + \alpha_1 v_4 = 0,\end{aligned} \tag{28a}$$

$$\begin{aligned}&\ddot{v}_3 + \omega_3^2 v_3 + \mu_3 V_W \dot{v}_2 + \mu_4 V_W \dot{v}_4\\ &-(p_3 u_m \cos\Omega_1 t)\, v_3 + \beta_3 v_3 v_2^2 + \beta_4 v_3^3\\ &-\alpha_2 (\bar{V} + V_m \sin\Omega_2 t)^2 = 0,\end{aligned} \tag{28b}$$

$$\ddot{v}_4 + \omega_4^2 v_4 + \mu_5 \dot{v}_4 = \alpha_3 (\bar{V} + V_m \sin\Omega_2 t)^2. \tag{28c}$$

Equation (28c) is a linear differential equation, and equations (28a) and (28b) are uncoupled. Therefore, the solution of Eq. (28c) can be substituted into the other two equations, thereby reducing the three-degree-of-freedom governing equation into a two-degree-of-freedom governing equation. According to the theory of forced vibration, the solution of Eq. (28c) yields

$$v_4 = B_0 + B_1 \sin\Omega_2 t + B_2 \cos 2\Omega_2 t, \tag{29}$$

where

$$B_0 = \frac{w_m^2 (2V^2 + V_m^2)}{2\omega_4^2}, \tag{30a}$$

$$B_1 = \frac{2w_m^2 (2VV_m)}{\sqrt{(\omega_4^2 - \Omega_2^2)^2 + 4\mu_4^2\Omega_2^2}}, \tag{30b}$$

$$B_2 = \frac{-w_m^2 (VV_m)}{2\sqrt{(\omega_4^2 - \Omega_2^2)^2 + 16\mu_4^2\Omega_2^2}}. \tag{30c}$$

Substitution of Eqs. (29) and (30) into Eqs. (28a) and (28b) yields the following equations:

$$\begin{aligned}&\ddot{v}_2 + \omega_2^2 v_2 + \mu_1 V_W \dot{v}_2\\ &+\mu_2 V_W (\Omega_2 B_1 \cos\Omega_2 t - 2\Omega_2 B_2 \sin 2\Omega_2 t)\\ &-(p_2 u_m \cos\Omega_1 t)\, v_2 + \beta_1 v_2 v_3^2 + \beta_2 v_2^3\\ &+\alpha_1 (B_0 + B_1 \sin\Omega_2 t + B_2 \cos 2\Omega_2 t) = 0,\end{aligned} \tag{31a}$$

$$\begin{aligned}&\ddot{v}_3 + \omega_3^2 v_3 + \mu_3 V_W \dot{v}_2\\ &+\mu_4 V_W (\Omega_2 B_1 \cos\Omega_2 t - 2\Omega_2 B_2 \sin 2\Omega_2 t)\\ &-(p_3 u_m \cos\Omega_1 t)\, v_3 + \beta_3 v_3 v_2^2\\ &+\beta_4 v_3^3 - \alpha_2 (\bar{V} + V_m \sin\Omega_2 t)^2 = 0.\end{aligned} \tag{31b}$$

By substituting the one-term expansion

$$v_2 = A_1 \sin(\omega t), \quad v_3 = A_2 \sin(\omega t) \tag{32}$$

into Eq. (31) and equating the coefficient of the harmonics to zero, an algebraic equation relating the frequency ω with the amplitudes A_1 and A_2 can be obtained.

3. Analysis of amplitude–frequency property

The introduction of a small perturbation parameter ε into Eq. (31) yields the following equations:

$$\begin{aligned}&\ddot{v}_2 + \omega_2^2 v_2 + \varepsilon\mu_1 \dot{v}_2\\ &+\varepsilon\mu_2 (\Omega_2 B_1 \cos\Omega_2 t - 2\Omega_2 B_2 \sin 2\Omega_2 t)\\ &-\varepsilon (p_2 u_m \cos\Omega_1 t)\, v_2 + \varepsilon\beta_1 v_2 v_3^2 + \varepsilon\beta_2 v_2^3\\ &+\varepsilon\alpha_1 (B_0 + B_1 \sin\Omega_2 t + B_2 \cos 2\Omega_2 t) = 0,\end{aligned} \tag{33a}$$

$$\begin{aligned}&\ddot{v}_3 + \omega_3^2 v_3 + \varepsilon\mu_3 \dot{v}_2\\ &+\varepsilon\mu_4 (\Omega_2 B_1 \cos\Omega_2 t - 2\Omega_2 B_2 \sin 2\Omega_2 t)\\ &-\varepsilon (p_3 u_m \cos\Omega_1 t)\, v_3 + \varepsilon\beta_3 v_3 v_2^2 + \varepsilon\beta_4 v_3^3\\ &-\varepsilon\alpha_2 (\bar{V} + V_m \sin\Omega_2 t)^2 = 0.\end{aligned} \tag{33b}$$

By the method of multiple scales, the following equations are obtained:

$$v_2(t,\varepsilon) = x_{20}(T_0, T_1) + \varepsilon x_{21}(T_0, T_1) + \cdots, \tag{34a}$$

$$v_3(t,\varepsilon) = x_{30}(T_0, T_1) + \varepsilon x_{31}(T_0, T_1) + \cdots, \tag{34b}$$

where $T_0 = t$ and $T_1 = \varepsilon t$.

The differential operator is

$$\frac{\mathrm{d}}{\mathrm{d}t} = \frac{\partial}{\partial T_0}\frac{\partial T_0}{\partial t} + \frac{\partial}{\partial T_1}\frac{\partial T_1}{\partial t} + \cdots = D_0 + \varepsilon D_1 + \cdots, \tag{35a}$$

$$\frac{\mathrm{d}^2}{\mathrm{d}t^2} = (D_0 + \varepsilon D_1 + \ldots)^2 = D_0^2 + 2\varepsilon D_0 D_1 + \cdots, \tag{35b}$$

where $D_k = \partial/\partial T_k$ and $k = 0, 1, \ldots$

Considering the case of principal parametric resonance, *i.e.*, 1/2 subharmonic resonance and 2:1 internal resonance, the following expressions are obtained:

$$\begin{aligned}&\Omega_1 = 2\Omega_2, \quad \omega_2^2 = \Omega_1^2 + \varepsilon\sigma_1,\\ &\omega_3^2 = \frac{\Omega_1^2}{4} + \varepsilon\sigma_2, \quad \omega_2 \approx 2\omega_3,\end{aligned} \tag{36}$$

where σ_1 and σ_2 are two detuning parameters, and $\Omega_1 = 2.0$.

By substituting Eqs. (33)–(35) into Eq. (32), the following equations are obtained:

$$\varepsilon^0: \quad D_0^2 x_{20} + 4x_{20} = 0, \tag{37a}$$

$$D_0^2 x_{30} + x_{30} = 0; \tag{37b}$$

$$\varepsilon^1: \quad D_0^2 x_{21} + 4x_{21} = -2D_0D_1x_{20} - x_{20}\sigma_1 - \mu_1 D_0 x_{20} - \mu_2\left(\Omega_2 B_1 \cos\Omega_2 t - 2\Omega_2 B_2 \sin 2\Omega_2 t\right) + \left(P_2 u_{\rm m}\cos\Omega_1 T_0\right)x_{20} - \beta_1 x_{20}x_{30}^2 - \beta_2 x_{20}^3 - \alpha_1\left(B_0 + B_1\sin\Omega_2 t + B_2\cos 2\Omega_2 t\right), \tag{38a}$$

$$D_0^2 x_{31} + x_{31} = -2D_0D_1x_{30} - x_{30}\sigma_2 - \mu_3 D_0 x_{20} - \mu_4\left(\Omega_2 B_1 \cos\Omega_2 t - 2\Omega_2 B_2 \sin 2\Omega_2 t\right) + \left(P_3 u_{\rm m}\cos\Omega_1 T_0\right)x_{30} - \beta_3 x_{30}x_{20}^2 - \beta_4 x_{30}^3 - \alpha_2\left(\bar{V} + V_{\rm m}\sin\Omega_2 t\right)^2. \tag{38b}$$

The polar form solution of Eq. (36) is

$$x_{20} = A_2(T_1)\,{\rm e}^{{\rm i}2T_0} + \bar{A}_2(T_1)\,{\rm e}^{-{\rm i}2T_0}, \tag{39a}$$

$$x_{30} = A_3(T_1)\,{\rm e}^{{\rm i}T_0} + \bar{A}_3(T_1)\,{\rm e}^{-{\rm i}T_0}, \tag{39b}$$

where $\bar{A}_i$ is the conjugate variable of A_i.

Substitute Eq. (39) into Eq. (38) and let the secular term be zero, then the following equations will be yielded:

$$-4D_1{\rm i}A_2 - \sigma_1 A_2 - 2{\rm i}\mu_1 A_2 - {\rm i}\mu_2 B_2 - 2\beta_1 A_3\bar{A}_3 A_2 - 3\beta_2 A_2^2\bar{A}_2 + \frac{1}{2}{\rm i}\alpha_1 B_2 = 0, \tag{40a}$$

$$-2D_1{\rm i}A_3 - \sigma_2 A_3 - \frac{1}{2}\mu_4 B_1 + \frac{1}{2}P_3 u_{\rm m}\bar{A}_3 - 2\beta_3 A_3\bar{A}_2 A_2 - 3\beta_4 A_3^2\bar{A}_3 + {\rm i}\alpha_2\bar{V}V_{\rm m} = 0. \tag{40b}$$

The averaged equation in the polar form of the iced suspended cable is derived as

$$2D_1A_2 = \frac{1}{2}{\rm i}\sigma_1 A_2 - \mu_1 A_2 - \frac{1}{2}\mu_2 B_2 + {\rm i}\beta_1 A_3\bar{A}_3 A_2 + \frac{3}{2}{\rm i}\beta_2 A_2^2\bar{A}_2 + \frac{1}{4}\alpha_1 B_2, \tag{41a}$$

$$2D_1A_3 = {\rm i}\sigma_2 A_3 + \frac{1}{2}{\rm i}\mu_4 B_1 - \frac{1}{2}{\rm i}P_3 u_{\rm m}\bar{A}_3 + 2{\rm i}\beta_3 A_3\bar{A}_2 A_2 + 3{\rm i}\beta_4 A_3^2\bar{A}_3 + \alpha_2\bar{V}V_{\rm m}. \tag{41b}$$

Let A_2 and A_3 be denoted in the following forms:

$$A_2(T_1) = \frac{1}{2}a_2\,{\rm e}^{{\rm i}\phi_2}, \quad \bar{A}_2(T_1) = \frac{1}{2}a_2\,{\rm e}^{-{\rm i}\phi_2}, \tag{42a}$$

$$A_3(T_1) = \frac{1}{2}a_3\,{\rm e}^{{\rm i}\phi_3}, \quad \bar{A}_3(T_1) = \frac{1}{2}a_3\,{\rm e}^{-{\rm i}\phi_3}, \tag{42b}$$

and substitute Eq. (42) into Eq. (41) and separate the real part and imaginary part, then the averaged equation in polar form will be obtained below.

$$\dot{a}_2 = -\frac{1}{2}\mu_1 a_2 + \left(\frac{1}{2}\mu_2 + \frac{1}{4}\alpha_1\right)B_2\cos\phi_2, \tag{43a}$$

$$a_2\dot{\phi}_2 = \frac{1}{4}\sigma_1 a_2 + \left(\frac{1}{2}\mu_2 + \frac{1}{4}\alpha_1\right)B_2\sin\phi_2 + \frac{1}{8}\beta_1 a_3^2 a_2 + \frac{3}{16}\beta_2 a_2^3, \tag{43b}$$

$$\dot{a}_3 = \frac{1}{2}\mu_4 B_1\sin\phi_3 - \frac{1}{4}P_3 u_{\rm m}a_3\sin(2\phi_3) + \alpha_2\bar{V}V_{\rm m}\cos\phi_3, \tag{43c}$$

$$a_3\dot{\phi}_3 = \frac{1}{2}\sigma_2 a_3 + \frac{1}{2}\mu_4 B_1\cos\phi_3 - \frac{1}{4}P_3 u_{\rm m}a_3\cos(2\phi_3) + \frac{3}{8}\beta_4 a_3^3 + \frac{1}{4}\beta_3 a_3 a_2^2 + \alpha_2\bar{V}V_{\rm m}\sin\phi_3. \tag{43d}$$

By equating the coefficients of sine and cosine in Eq. (43) to zero, the relationship between the amplitude–frequency characteristics is obtained as follows:

$$\left(\frac{1}{2}\mu_1 a_2\right)^2 + \left(\frac{1}{4}\sigma_1 a_2 + \frac{1}{8}\beta_1 a_3^2 a_2 + \frac{3}{16}\beta_2 a_2^3\right)^2 = \left(\frac{1}{2}\mu_2 + \frac{1}{4}\alpha_1\right)^2 B_2^2, \tag{44a}$$

$$\left(\frac{1}{2}\sigma_2 a_3 + \frac{3}{8}\beta_4 a_3^3 + \frac{1}{4}\beta_3 a_3 a_2^2\right)^2 + \left(\frac{1}{2}\mu_4 B_1\right)^2 = \left(-\frac{1}{4}P_3 u_{\rm m}a_3 + \alpha_2\bar{V}V_{\rm m}\right)^2. \tag{44b}$$

To study the complex dynamics of the iced cable, the amplitude–frequency characteristics curves of system (31) are analyzed. However, the analytical solutions of system (31) are very difficult to obtain; therefore, the following two special cases are considered:

(i) the two modes are weakly coupled;

(ii) the two modes are strongly coupled.

For case (i), assume $a_3 = 1$ in Eq. (44a) and $a_2 = 1$ in Eq. (44b), then the amplitude–frequency relationship of the weakly coupled system will be expressed as

$$\left(\frac{1}{2}\mu_1 a_2\right)^2 + \left(\frac{1}{4}\sigma_1 a_2 + \frac{1}{8}\beta_1 a_2 + \frac{3}{16}\beta_2 a_2^3\right)^2 = \left(\frac{1}{2}\mu_2 + \frac{1}{4}\alpha_1\right)^2 B_2^2, \tag{45a}$$

$$\left(\frac{1}{2}\sigma_2 a_3 + \frac{3}{8}\beta_4 a_3^3 + \frac{1}{4}\beta_3 a_3\right)^2 + \left(\frac{1}{2}\mu_4 B_1\right)^2 = \left(-\frac{1}{4}P_3 u_{\rm m}a_3 + \alpha_2\bar{V}V_{\rm m}\right)^2. \tag{45b}$$

Figures 2 and 3 respectively present the amplitudes a_2 and a_3 *versus* detuning parameter σ_1 and B_2 under different values of damping coefficient μ_1. The results demonstrate that the increase of the damping coefficient μ_1 will lead to the decrease in the amplitudes a_2 and a_3. Moreover, figures 2 and 3 present the hardening properties of the stiffness and jump phenomenon of the amplitude based on the amplitude–frequency curve.

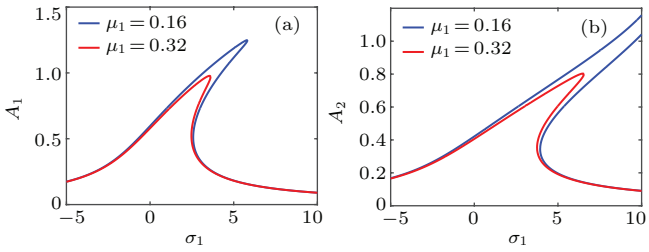


Fig. 2. Weak coupling amplitude–frequency (a) A_1 and (b) A_2 *versus* σ_1 under different damping coefficients.

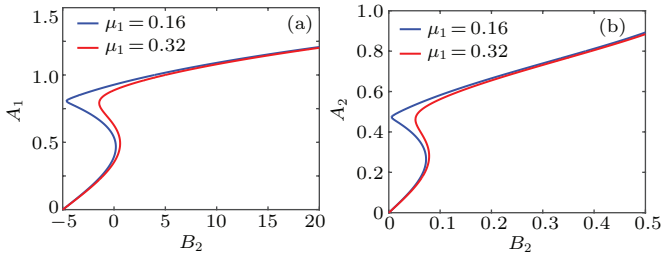


Fig. 3. Weak coupling amplitude–frequency (a) A_1 and (b) A_2 *versus* B_2 under different damping coefficients.

For case (ii), assume $a_3 = 2$ in Eq. (44a) and $a_2 = 2$ in Eq. (44b), then the strongly coupled system will be obtained as follows:

$$\left(\frac{1}{2}\mu_1 a_2\right)^2 + \left(\frac{1}{4}\sigma_1 a_2 + \frac{1}{2}\beta_1 a_2 + \frac{3}{16}\beta_2 a_2^3\right)^2 = \left(\frac{1}{2}\mu_2 + \frac{1}{4}\alpha_1\right)^2 B_2^2, \tag{46a}$$

$$\left(\frac{1}{2}\sigma_2 a_3 + \frac{3}{8}\beta_4 a_3^3 + \beta_3 a_3\right)^2 + \left(\frac{1}{2}\mu_4 B_1\right)^2 = \left(-\frac{1}{4}P_3 u_m a_3 + \alpha_2 \bar{V} V_m\right)^2. \tag{46b}$$

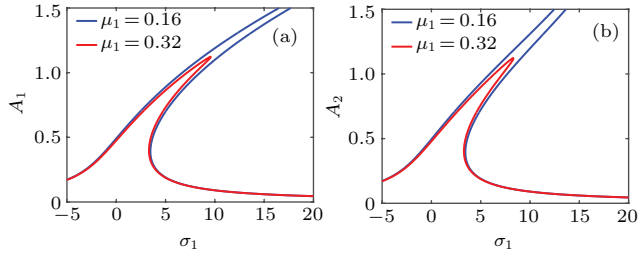


Fig. 4. Strong coupling amplitude-frequency (a) A_1 and (b) A_2 *versus* σ_1 under different damping coefficients.

Figures 4 and 5 respectively present the amplitudes a_2 and a_3 *versus* detuning parameters σ_1 and B_2 under different values of damping coefficient μ_1. Like case (i), with the increase of the damping coefficient μ_1, the amplitudes a_2 and a_3 decrease. In addition, with the constant change of parameters, the amplitude of the system will present a jump phenomenon. It can be seen that the amplitudes in case (ii) are larger than those in case (i), which is due to the differences between the two cases.

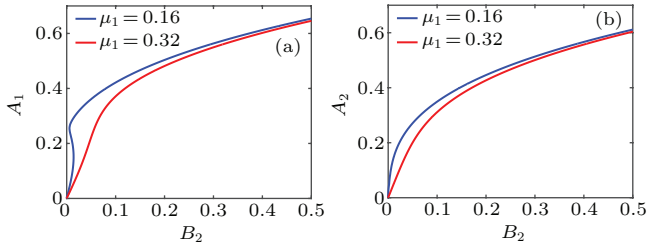


Fig. 5. Strong coupling amplitude–frequency (a) A_1 and (b) A_2 *versus* B_2 under different damping coefficients.

4. Numerical simulations of periodic and chaotic motions

Numerical simulations are performed to determine the periodic motion and chaotic motion of the iced suspended cable. The numerical integration of Eq. (31) is performed by using the Runge–Kutta algorithm with variable precision $\in [0.0001, 0.01]$.[38] More specifically, the transient effects are avoided by dropping the first 60% of the simulating time: 2000 s. The excitation V is a main controlling parameter in the research of the nonlinear dynamic behaviors of cables, and is selected as the controlling parameter to discover the complicated nonlinear dynamics. The parameters are set to be as follows: $E = 0.9 \times 10^{11}$ Pa, $G = 0.4 \times 10^{11}$ Pa, $g = 9.8$ N/kg, $L = 400$ m, $\rho = 0.92$ kg/m, $\rho_{\text{air}} = 1.2$ kg/m^3, $R = 10 \times 10^{-3}$ m, and $u_m = 1$ m.

In this section, the emphasis is placed on the influence of external excitation on the motion of a three-degree-of-freedom iced suspended cable structure. The horizontal wind speed V is taken as the control parameter. The amplitude of the wind speed pulse is constant, and the amplitude u_m of the bearing motion is assumed to be a constant value. The dependence of the three-degree-of-freedom iced cable on the horizontal wind speed V is investigated. Considering the parametric and external excitation on the iced cable, there exist abundant dynamic behaviors. The dynamic motions of the iced cable under different wind speeds are calculated based on the torsional vibration of the three-degree-of-freedom system which occurs in a single cycle. Table 1 exhibits the typical examples of the motion forms of the iced cable under different wind speeds. The bifurcation diagrams of the two degrees of freedom v_2 and v_3 *versus* wind speed V are presented in Figs. 6(a) and 6(b), respectively and figure 6(c) shows the largest Lyapunov exponent of v_2. When $V \in [0.78, 0.88]$, $V \in [1.36, 1.75]$, and $V > 1.9$, the system exhibits the typical characteristics of chaotic motion.

Table 1. Typical examples of motion forms of iced cable under different wind speeds.

Horizontal wind speed (m/s)	Motion of the system
$V = 0.83$	period-1 motion
$V = 0.94$	multi-period motion
$V = 1.01$	quasi-periodic motion
$V = 1.17$	chaotic motion

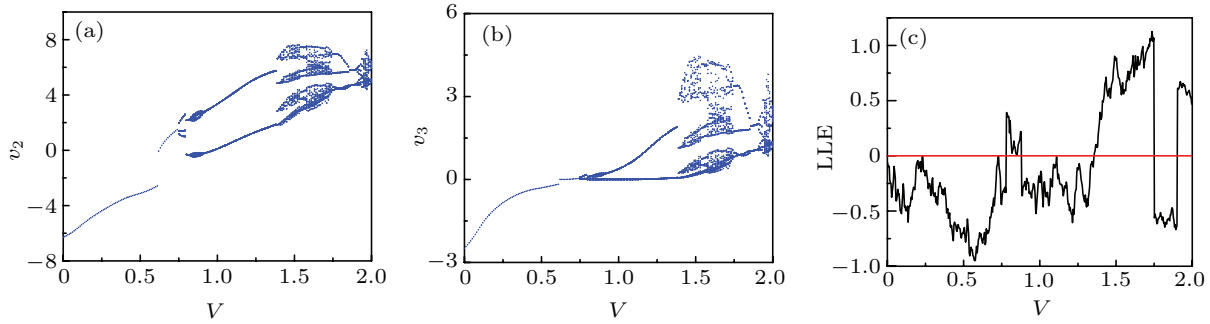


Fig. 6. Bifurcation diagram of v_2 and v_3 under different values of wind speed V_1.

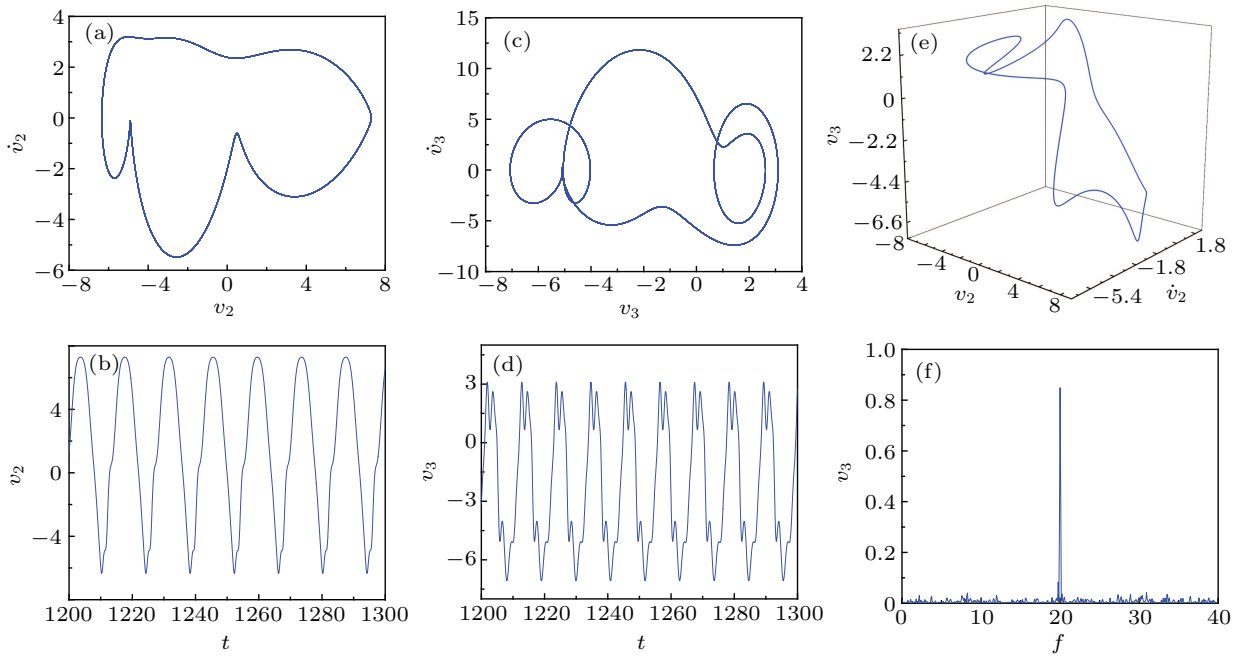


Fig. 7. Periodic motion of iced cable obtained when $V = 0.83$ m/s.

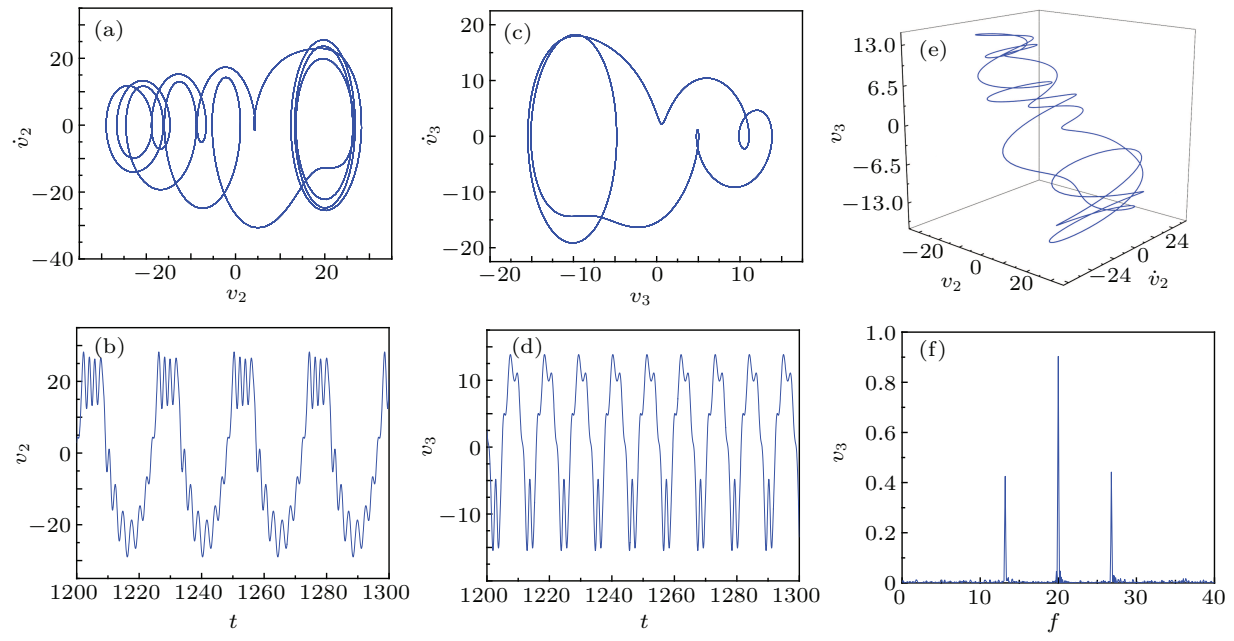


Fig. 8. Multi-periodic motion of iced cable obtained when $V = 0.94$ m/s.

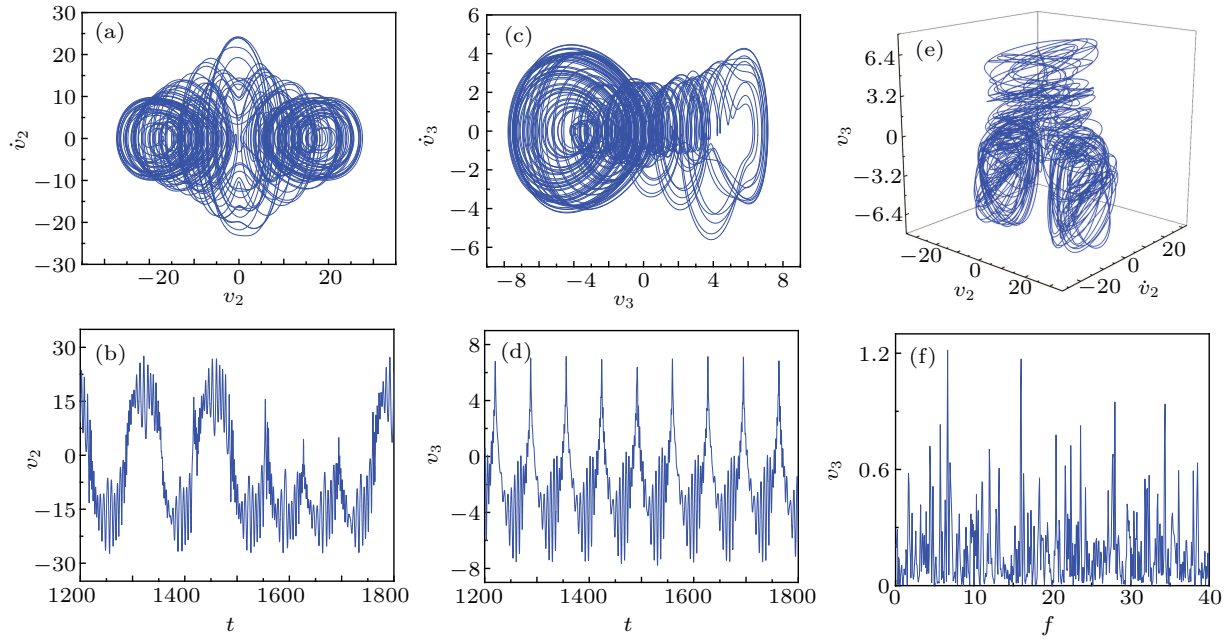


Fig. 9. Chaotic motion of iced cable obtained when $V = 1.17$ m/s.

In each of Figs. 7–9, panels (a) and (c) respectively show the phase portraits on the planes $(v_2, \dot{v}_2)$ and $(v_3, \dot{v}_3)$, panels (b) and (d) respectively represent the waveforms on the planes (t, v_2) and (t, v_3), and panels (e) and (f) respectively display the three-dimensional phase portrait in space $(v_2, \dot{v}_2, v_3)$ and the frequency spectrum on plane (frequency, v_2). It should be noted that the frequency spectrum can be used to distinguish between periodic motion and chaotic motion. The results reveal that there exist one-periodic motion (Fig. 7), multi-periodic motion (Fig. 8), and chaotic motion (Fig. 9) when the system is under the action of different resonance mechanisms, including in-plane parametric resonance and out-of-plane superharmonic resonance. Moreover, the displacement of the vibration is found to be enhanced with the increase of the wind speed.

5. Conclusions

In this paper, the theory of nonlinear dynamics is used to investigate the wind-excited vibration response of an iced suspended cable. The effects of the system under both external and parametric excitation are investigated. Using Hamilton's principle, a dynamic model of a three-degree-of-freedom iced suspended cable is first established. Then, the approximate equation in the case of small sag is derived, as shown in the dimensionless equation. The amplitude–frequency characteristics are obtained using the harmonic balance method. The perturbation equation is analyzed using the method of multiple scales, and the averaged equation is derived and used to capture the behaviors of the system under the action of in-plane parametric resonance and out-of-plane superharmonic resonance. Based on the numerical simulation, the nonlinear vibration responses of the iced cable under parametric excitation and external excitation caused by horizontal wind are determined. The numerical results reveal that the iced suspended cable presents a periodic motion, multi-periodic motion, and chaotic motion under in-plane parametric resonance and out-of-plane main resonance. It is found that with the increase of the wind speed, the behavior of the system changes from a one-periodic motion into a multi-periodic motion, and finally into a chaotic motion. Compared with the results of a two-degree-of-freedom iced suspended cable, the effect of torsional vibration on the system cannot be neglected. Furthermore, theoretical analysis reveals that the vibration of the iced cable can be effectively controlled, which could be a useful technique to ensure the safety of the cable structure.

References

[1] Irvine H M and Caughey T K 1974 *P. Roy. Soc. A - Math. Phys.* **341** 299
[2] Starossek U 1994 *Struct. Eng. Int.* **4** 171
[3] Rega G 2004 *Appl. Mech. Rev.* **57** 443
[4] Rega G 2004 *Appl. Mech. Rev.* **57** 479
[5] Ibrahim R A 2004 *Appl. Mech. Rev.* **57** 515
[6] Perkins N C 1992 *Int. J. Nonlinear Mech.* **27** 233
[7] Benedettini F, Rega G and Alaggio R 1995 *J. Sound Vib.* **182** 775
[8] Gattulli V, Martinelli L, Perotti F and Vestroni F 2004 *Comput. Method Appl. M* **193** 69
[9] Luongo A, Zulli D and Piccardo G 2009 *Comput. Struct.* **87** 1003
[10] Luongo A, Zulli D and Piccardo G 2008 *J. Sound Vib.* **315** 375
[11] Luongo A, Paolone A and Piccardo G 1998 *Meccanica* **33** 229
[12] Kim W J and Perkins N C 2002 *J. Fluid Struct.* **16** 229
[13] Srinil N, Rega G and Chucheepsakul S 2003 *Nonlinear Dyn.* **33** 129
[14] Zhao Y and Wang L 2006 *J. Sound Vib.* **294** 1073
[15] Casciati F and Ubertini F 2008 *Nonlinear Dyn.* **53** 89
[16] Abdel-Rohman M and Spencer B F 2004 *Nonlinear Dyn.* **37** 341
[17] Zheng G J, Ko M and Ni Y Q 2002 *Nonlinear Dyn.* **30** 55
[18] Chang W K, Pilipchuk V and Ibrahim R A 1997 *Nonlinear Dyn.* **14** 377

[19] Ouni M H E and Kahla N B 2012 *J. Civ. Eng. Manag.* **18** 557
[20] Zhao Y, Sun C, Wang Z and Wang L 2014 *Shock Vib.* **2014** 795708
[21] Zhao Y, Sun C, Wang Z and Wang L 2014 *Nonlinear Dyn.* **78** 1017
[22] Srinil N, Rega G and Chucheepsakul S 2007 *Nonlinear Dyn.* **48** 231
[23] Srinil N and Rega G 2007 *Nonlinear Dyn.* **48** 253
[24] Nayfeh A H, Arafat H N, Chin C M and Lacarbonara W 2002 *Modal Analysis* **8** 337
[25] Lacarbonara W and Rega G 2003 *Int. J. Nonlinear Mech.* **38** 873
[26] Kamel M M and Hamed Y S 2002 *Acta Mech.* **214** 315
[27] Rega G, Alaggio R and Benedettini F 1997 *Nonlinear Dyn.* **14** 89
[28] Zhang W and Tang Y 2002 *Int. J. Nonlinear Mech.* **37** 505
[29] Wu Q L, Zhang W and Dowell E H 2018 *Int. J. Nonlinear Mech.* **102** 25
[30] Wu Q L and Qi G Y 2019 *Phys. Lett. A* **383** 1555
[31] Wu Q L and Qi G Y 2020 *Appl. Math. Model.* **83** 674
[32] Abe A 2010 *Nonlinear Anal. - Real.* **11** 2594
[33] Huang K, Feng Q and Yin Y 2014 *Acta Mech. Solida Sin.* **27** 467
[34] Kang H J, Zhao Y Y and Zhu H P 2015 *J. Vib. Control* **21** 1487
[35] Kang H J, Guo T D, Zhao Y Y, Fu W B and Wang L H 2017 *Eur. J. Mech. A - Solid* **62** 94
[36] Wei M H, Lin K, Jin L and Zou D J 2016 *Int. J. Mech. Sci.* **110** 78
[37] Wu Q L and Qi G Y 2020 *Eur. J. Mech. A - Solid* **82** 104012
[38] Jing H, He X and Wang Z 2018 *J. Fluid Struct.* **82** 121
[39] Górski P, Pospíšil S, Tatara M and Trush A 2019 *J. Wind Eng. Ind. Aerod.* **191** 297
[40] Zhao Y L, Xu Z D and Wang C 2019 *J. Sound Vib.* **443** 732
[41] Chang Y, Zhao L and Ge Y 2019 *J. Fluid Struct.* **88** 257
[42] Li Y, Shen W and Zhu H 2019 *Eng. Struct.* **200** 109693
[43] Huang K, Feng Q and Qu B 2017 *Nonlinear Dyn.* **87** 2765
[44] Ahmad J, Cheng S and Ghrib F 2018 *J. Sound Vib.* **417** 132
[45] Ishihara T and Oka S 2018 *J. Wind Eng. Ind. Aerod.* **177** 60
[46] Akkaya T and Horssen W T V 2019 *Nonlinear Dyn.* **95** 783
[47] Javanbakht M, Cheng S and Ghrib F 2019 *J. Sound Vib.* **442** 249
[48] Li M. Li M. Zhong Y and Luo N 2019 *J. Sound Vib.* **439** 156
[49] Guo T, Kang H, Wang L and Zhao Y 2017 *Nonlinear Dyn.* **90** 1941
[50] Mansour A, Mekki O B, Montassar S and Rega G 2018 *J. Sound Vib.* **413** 332
[51] Zhao Y, Peng J, Zhao Y and Chen L 2017 *Nonlinear Dyn.* **89** 2815
[52] Zhao Y, Huang C, Chen L and Peng J 2018 *J. Sound Vib.* **416** 279
[53] Wu Q L and Qi G Y 2021 *Appl. Math. Model.* **90** 1120
[54] Wu Q L, Yao M H, Li M Y, Cao D X and Bai B 2021 *Appl. Math. Model.* **93** 75